ChemComm

COMMUNICATION

View Article Online
View Journal | View Issue

Cite this: *Chem. Commun.*, 2025, **61**, 18721

Received 17th September 2025,
Accepted 22nd October 2025

DOI: 10.1039/d5cc05347a

rsc.li/chemcomm

Olefin insertion using *ansa*-zirconocenes and methylaluminoxane (MAO) involves Janus-like, sheet anions

Munmun Bharti, Aleksi Vähäkangas, Mikko Linnolahti* and Scott Collins*

Two isomeric contact ion-pairs *rac*-$Me_2Si(\eta^5\text{-}C_9H_6)_2ZrMe\text{-}\mu\text{-}Me\text{-}(MeAlO)_{16}(Me_3Al)_6$ (1a and 1b), differing only in the detailed structure of the sheet counter-anion, are the active species in zirconocene-catalyzed olefin polymerization, mediated by methylaluminoxane (MAO), the most industrially important activator. Theoretical studies of novel, sheet models for the most abundant anion $[(MeAlO)_{16}(Me_3Al)_6Me]^-$ detected in mixtures of MAO and metallocene complexes show that the propene insertion barriers for 1a and 1b have large differences with the more reactive species 1a having insertion barriers in good agreement with experiments. The reactivity of these isomeric ion-pairs would vary by more than two-orders of magnitude and has important implications for polymerization catalysis.

Ever since its discovery as an effective co-catalyst for metallocene-catalyzed olefin polymerization, methylaluminoxane (MAO)[1] has attracted widespread industrial and scientific interest as to its structure and mechanism of action.[2] This catalyst system enables production of the polyolefin plastics found in everyday items, representing a market share approaching $10 billion annually.

A large excess of MAO reacts with metallocene complexes, *e.g.* *rac*-$Me_2Si(\eta^5\text{-}C_9H_6)_2ZrMe_2$ ($SBIZrMe_2$), to furnish at least two ion-pairs **1** and **2**,[3] and these are the active and dormant species,[4] respectively, involved in olefin polymerization (Scheme 1). Though the structure of the cationic portion in ion-pairs **1** and **2** has never been in doubt,[5] the structure of the activators[6] and the counter-anion(s)[7] have defied experiment for decades and hinder further improvements to this important activator.

Recent experimental progress towards this goal has relied on ESI-MS detection of the anions and cations formed from metallocenes and MAO in fluorobenzene,[8,9] where the most abundant anion has the composition $[(MeAlO)_{16}(Me_3Al)_6Me]^-$ ($[16,6]^-$), as deduced from MS–MS experiments.[10] More recently, a minor, but reactive component isolated from a mixture of MAO and octamethyltrisiloxane (OMTS), *viz* $(MeAlO)_{26}(Me_3Al)_9$ (26,9) has been structurally characterized and adopts a sheet structure (Fig. 1).[11] Furthermore, a subsequent X-ray scattering study revealed that bulk MAO likely consists of sheets, which can aggregate.[12] Most recently, the structure of bulk *vs.* active Al sites in MAO and Cp_2ZrMe_2 contact ion-pairs (CIPs), analogous to **1**, at low Al:Zr ratios was clarified using ultra-high field, solid state ^{27}Al NMR spectroscopy.[13]

Although accumulating theoretical work has indicated that sheets are stable components of MAO,[14] the lowest energy sheet model located for the $[16,6]^-$ anion[15] when partnered with the $[SBIZrMe]^+$ cation to form CIP **1** exhibited propene insertion barriers[16] that were far too high in comparison to experiments.[17,18]

Also, recent work on the reaction of aluminoxane sheet models of different size with OMTS[19] revealed that the stable 16,6 model[20] was the least reactive precursor towards the formation of $[Me_2Al(OMTS)][n,m]$ outer-sphere ion-pairs (OSIP) in fluorobenzene, in disagreement with experimental results.[10]

In this communication, we present a new, more stable sheet model for the $[16,6]^-$ anion (Fig. 1), located using topological analysis of infinite MAO sheets.[21] We show that this anion is

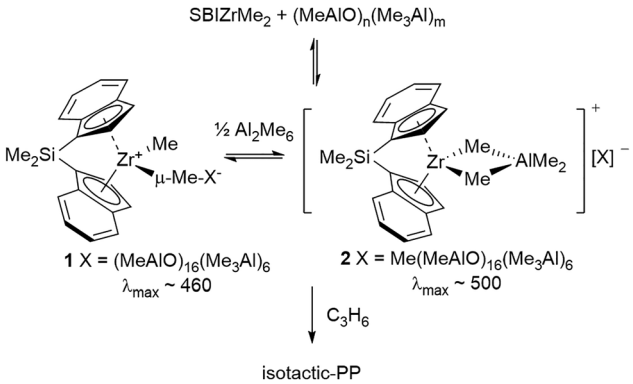

Scheme 1 Activation of *rac*-$Me_2Si(\eta^5\text{-}C_9H_6)_2ZrMe_2$ by MAO.

Department of Chemistry and Sustainable Technology, University of Eastern Finland, Joensuu Campus, Yliopistokatu 7, FI-80100, Joensuu, Finland. E-mail: mikko.linnolahti@uef.fi, scottcol@uef.fi

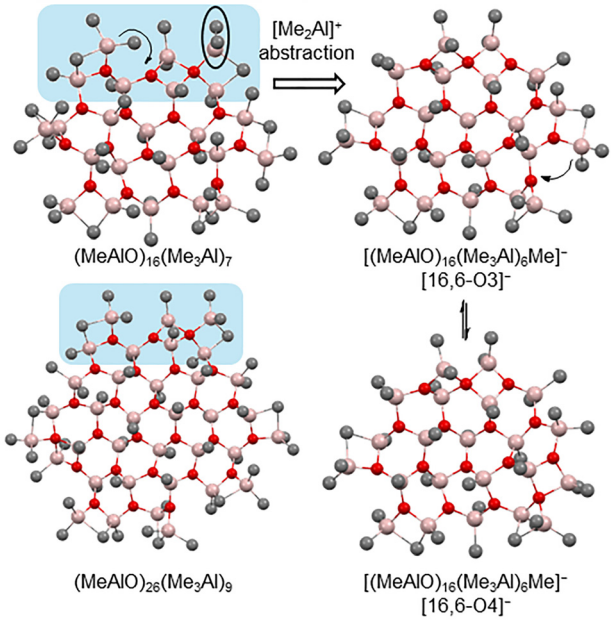

Fig. 1 Neutral sheet 16,7 compared to the isolated 26,9 sheet and the corresponding isomeric anions $[16,6]^-$ (right) formed by $[Me_2Al]^+$ abstraction. Al atoms in pink, O in red, and C in gray with H-atoms omitted for clarity.

indeed weakly coordinating and when paired with a prototypical metallocenium ion (*i.e.* **1**) forms an active polymerization catalyst in agreement with experiments. Surprisingly, almost identical isomers of this new sheet anion (Fig. 1) differ in catalytic reactivity by more than 1000-fold—one is an active catalyst while the other is essentially dormant. Such dramatic differences from subtle structural changes are very unusual and unexpected, further highlighting the mysterious nature of this industrially important cocatalyst.[2]

The new reactive precursor was located by systematic cuts of an infinite MAO sheet, with an optimal up *vs.* down arrangement of methyl groups, analogous to the alternating hydrogen pattern in graphane, the hydrogenated form of graphene.[22] Full details will be reported elsewhere,[23] but the most stable activator $(MeAlO)_{16}(Me_3Al)_7$ (16,7) features the ovalene-like framework while the edges feature reactive sites identified in other aluminoxane sheets (including our original model for the 16,6 precursor) and the larger, structurally characterized 26,9 sheet. In fact, the neutral 16,7 sheet mimics one reactive portion of this larger sheet as shown in Fig. 1 (highlighted in blue).

A stable $[16,6\text{-O3}]^-$ anion, close to 40 kJ mol^{-1} lower in E than our original $[16,6]^-$ sheet anion, results from $[Me_2Al]^+$ abstraction from this precursor at the site indicated. This anion can adopt several configurations differing in the number of tetra- *vs.* tri-coordinate O atoms present along the sheet edges (*e.g.* Fig. 1). Calculations at the M06-2X,[24] RI-MP2[25] and DLPNO-CCSD(T)[26] levels (Table S-1) reveal that the most stable anion (O3) adopts the structure where all but one of the oxygen atoms are three-coordinate, though the other isomer is within 10 kJ mol^{-1} of this one, and with very low barriers to interconversion (ΔE = 8.3 kJ mol^{-1} at 298 K at M06-2X level). As discussed elsewhere,[19] DFT predicts the relative energy of these isomers incorrectly, as this theory anomalously favours 4- over 3-coordinate O, with $[16,6\text{-O4}]^-$ being lower in E than $[16,6\text{-O3}]^-$ but only by 7.7 kJ mol^{-1} at the M06-2X level of theory.

CIP **1a-b** involving the $[SBIZrMe]^+$ cation were located by docking this species to each of the O3 and O4 anions at the most electron rich $AlMe_2$ groups as described earlier.[27] We used the M06L[24]/SV(P)[28] theory as implemented within ORCA 6.0[29] to locate/rank these structures from amongst several isomers based on E. *syn*-π-C_3H_6-complexes **3a-b**, insertion transition structures **4a-b**, γ-agostic insertion products **5a-b** and homologated CIP **6a-b** were then located using the same approach with final optimizations in the toluene continuum[30] using both the M06-2X/TZVP[31] and MN15[32]/def2-TZVP[28] methods as implemented in Gaussian 16.[33] Analogous gas phase calculations on SBIZrMe-μ-Me-B$(C_6F_5)_3$ (**1c**),[16] SBIZrMe(μ-F-$C_6F_4B(C_6F_5)_3$) (**1d**),[16] and SBIZrMe-μ-Me-26,8 (**1e**),[27] CIP **1a-b** and the corresponding transition structures **4a-b** involved in insertion were supplemented by RI-MP2 and DLPNO-CCSD(T) calculations on these very large structures. This work showed that M06-2X correctly predicted the large difference between electronic insertion barriers for **1a** and **1b** at the CCSD(T) level while providing reasonable free energy barriers for the other ion-pairs, compared to experiments (SI, Table S-2).

Surprisingly, with the new $[16,6]^-$ sheet models, the insertion barrier was a strong function of the O3 *vs.* O4 configuration of both the precursors, the intermediates, and the transition

Table 1 Insertion energetics for SBIZr ion-pairs and new sheet models for the $[16,6]^-$ anion[a]

Structure[b]	ΔE	ΔH-qh	$T\Delta S$-qh-tr	ΔG-qh-tr[c]
SBIZrMe-μ-Me-16,6-O3 **1a** + C_3H_6	0.0	0.0	0.0	0.0
syn-[SBIZrMe(π-C_3H_6)][16,6-O3] **3a**	−15.4	−8.3	−31.4	23.1
syn-[SBIZr(C_4H_9)][16,6-O3] TS **4a**	20.7	27.2	−40.3	67.5
syn-[SBIZr(C_4H_9)][16,6-O3] γ-CH **5a**	−40.9	−27.1	−42.4	15.3
SBIZr(i-Bu)-μ-Me-16,6-O3 **6a**	−99.2	−83.8	−41.2	−42.6
SBIZrMe-μ-Me-16,6-O4 **1b** + C_3H_6	0.0	0.0	0.0	0.0
syn-[SBIZrMe(π-C_3H_6)][16,6-O4] **3b**	5.3	10.7	−35.9	46.6
syn-[SBIZr(C_4H_9)][16,6-O4] TS **4b**	43.4	48.4	−44.8	93.2
syn-[SBIZr(C_4H_9)][16,6-O4] γ-CH **5b**	−16.7	−5.3	−44.2	38.9
SBIZr(i-Bu)-μ-Me-16,6-O4 **6b**	−105.7	−89.9	−47.3	−42.6

[a] Energies (kJ mol^{-1}) at the M06-2X/TZVP level in the toluene polar continuum are given relative to ion-pair **1a** or **1b** + C_3H_6. [b] For coordinates see SI, Table S-1.xyz. [c] Enthalpy,[35] entropy[36] and free energy corrected using a quasi-harmonic approximation for low energy vibrations[37] and for the reduced translational entropy in the condensed phase.[38]

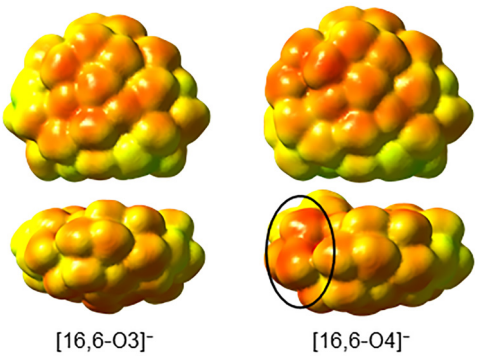

Fig. 2 Electrostatic potentials of the [16,6]⁻ anions show significant differences in electron density (red *vs.* yellow/green). An electron rich $AlMe_2$ group is highlighted in the more coordinating [16,6-O4]⁻ anion.

structures. This is shown in Table 1, which summarizes the energetic data at the M06-2X level in the toluene continuum (for the reaction profile, see SI). The DLPNO-CCSD(T) calculations indicate that the electronic insertion barriers determined using M06-2X for **1a** and **1b** are too high by 6.8 and 10.0 kJ mol^{-1}, respectively. This means that our corrected estimates for the insertion barriers are $\Delta G^{\ddagger}$-qh-tr = 83.2 kJ mol^{-1} for **1b** *vs.* only 60.7 kJ mol^{-1} for **1a**. The $T\Delta S$ values vary between $\sigma = \pm 5.0$ kJ mol^{-1} at 298 K for **1a** and **1b** (Table 1). The differences in $\Delta G^{\ddagger}$-qh-tr are well outside the variation in $T\Delta S$ values,[34] indicating a catalyst system whose reactivity could vary by more than two orders of magnitude.

The dramatic difference in reactivity can be explained by comparing electrostatic potential maps of these anions. The O3 anion (Fig. 2) shows significantly enhanced charge delocalization compared with the O4 anion.

The O4 anion forms more stable CIP with the electron-rich $AlMe_2$ group (circled), essentially trapping the metallocene in a less reactive state. We suspect that this is the root cause of the large energy differences, as the two faces of the sheet anions, which interact with the cation in OSIP such as **3** or **4**, are not as different (SI, Fig. S-1).

It is fascinating to contemplate these results in the context of a propagating catalyst (Fig. 3). There is a modest E difference between the homologated ion-pairs **6** favoring **6b**, which is offset by the higher entropy of the O3 *vs.* O4 configuration.[23] Thus, CIP **6a** and **6b** (also **1a** and **1b**) will be present in comparable amounts. These isomers cannot easily interconvert as Zr is coordinated to two different $AlMe_2$ groups. Isomer **6b** (or **1b**) would be dormant compared with the other with respect to processes competing with insertion.[39,40] However, any OSIP formed reversibly from these species—in order of decreasing stability, complexes **2** (see SI), the π complexes **3** or a toluene solvate[41] could undergo facile isomerization as with the anions (Fig. 1). Thus, this two-state catalyst might simply have reduced active site concentrations[17] as part of the catalyst pools in the dormant state.

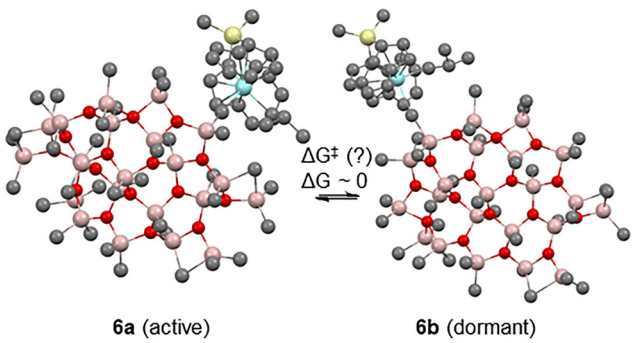

Fig. 3 A two state metallocene catalyst differing in only the detailed structure of the counter-anion.

Future work will address these issues in the context of catalyst speciation during both catalyst activation and propagation. Also, the findings here do not explain why the activity of the MAO-based systems in solution is a sensitive function of the Al : Zr ratio used for catalyst activation.[27] However, based on the work presented here, the major, reactive species in $SBIZrMe_2$-MAO-catalyzed olefin polymerization has the structure shown in Fig. 3 for **6a**.

M. B. and M. L. acknowledge the financial support of the Research Council of Finland, decision 357509. A. V. acknowledges the financial support of the Finnish Ministry of Education and Culture through the I-DEEP Doctoral Education Pilot Program. S. C. acknowledges the University of Eastern Finland for a Visiting Scientist position. The authors acknowledge CSC – IT Center for Science, Finland, and Finnish Grid and Cloud Infrastructure (urn:nbn:fi:research-infras-2016072533) for computational resources.

Conflicts of interest

There are no conflicts to declare.

Data availability

The data supporting this article have been included as part of the supplementary information (SI). Supplementary information: computational details, tables of electronic energies and a figure comparing electrostatic potential surfaces of anions. Atomic coordinates and electronic energies deposited to Table S-1.xyz. See DOI: **https://doi.org/10.1039/d5cc05347a**.

References

1 W. Kaminsky, *Macromolecules*, 2012, **45**, 3289–3297.
2 H. S. Zijlstra and S. Harder, *Eur. J. Inorg. Chem.*, 2015, 19–43.
3 U. Wieser, F. Schaper and H. H. Brintzinger, *Macromol. Symp.*, 2006, **236**, 63–68.
4 D. E. Babushkin and H. H. Brintzinger, *J. Am. Chem. Soc.*, 2010, **132**, 452–453.
5 M. Bochmann, *Organometallics*, 2010, **29**, 4711–4740.
6 E. Y.-X. Chen and T. J. Marks, *Chem. Rev.*, 2000, **100**, 1391–1434.
7 F. Zaccaria, L. Sian, C. Zuccaccia and A. Macchioni, in *Advances in Organometallic Chemistry*, ed. P. J. Perez, Academic Press, Cambridge MA, 2020, ch. 1, vol. 73, pp. 1–78.
8 S. Collins and M. Linnolahti, *ChemCatChem*, 2022, **14**, e202101918.
9 T. K. Trefz, M. A. Henderson, M. Linnolahti, S. Collins and J. S. McIndoe, *Chem. – Eur. J.*, 2015, **21**, 2980–2991.

10 H. S. Zijlstra, M. Linnolahti, S. Collins and J. S. McIndoe, *Organometallics*, 2017, **36**, 1803–1809.
11 L. Luo, J. M. Younker and A. V. Zabula, *Science*, 2024, **384**, 1424–1428.
12 T. Wada and T. Taniike, *Nanoscale*, 2025, **17**, 6767–6779.
13 K. Szeto, M. Taoufik, F. Fayon, D. Gajan, E. Zurek, J. Autschbach, J. Trébosc, L. Delevoye and R. M. Gauvin, *Angew. Chem., Int. Ed.*, 2025, **64**, e202508409.
14 M. Linnolahti and S. Collins, *ChemPhysChem*, 2017, **18**, 3369–3374.
15 A. Joshi, H. S. Zijlstra, E. Liles, C. Concepcion, M. Linnolahti and J. S. McIndoe, *Chem. Sci.*, 2021, **12**, 546–551.
16 S. Collins and M. Linnolahti, *ChemPhysChem*, 2024, **25**, e202300856.
17 F. Song, R. D. Cannon and M. Bochmann, *J. Am. Chem. Soc.*, 2003, **125**, 7641–7653.
18 J. Zhou, S. J. Lancaster, D. A. Walker, S. Beck, M. Thornton-Pett and M. Bochmann, *J. Am. Chem. Soc.*, 2001, **123**, 223–237.
19 X. Mao, M. Bharti, S. Collins and M. Linnolahti, *Chem. – Eur. J.*, 2025, **31**, e202404642.
20 A. Joshi, S. Collins, M. Linnolahti, H. S. Zijlstra, E. Liles and J. S. McIndoe, *Chem. – Eur. J.*, 2021, **27**, 8753–8763.
21 M. Linnolahti, T. N. P. Luhtanen and T. A. Pakkanen, *ChemPhysChem*, 2004, **10**, 5977–5987.
22 J. O. Sofo, A. S. Chaudhari and G. D. Barber, *Phys. Rev. B: Condens. Matter Mater. Phys.*, 2007, **75**, 153401.
23 M. Bharti, A. Vähäkangas, P. Hanhisalo, S. Collins and M. Linnolahti, *ChemRxiv*, 2025, preprint, chemrxiv-2025-8g0gd, Inorg. Chem. Frontiers submitted for publication, DOI: **10.26434/chemrxiv-2025-8g0gd**.
24 Y. Zhao and D. G. Truhlar, *Theor. Chem. Acc.*, 2008, **120**, 215–241.
25 F. Weigend, M. Häser, H. Patzelt and R. Ahlrichs, *Chem. Phys. Lett.*, 1998, **294**, 143–152.
26 C. Riplinger, B. Sandhoefer, A. Hansen and F. Neese, *J. Chem. Phys.*, 2013, **139**, 134101.
27 S. Collins and M. Linnolahti, *Dalton Trans.*, 2025, **54**, 2331–2339.
28 F. Weigend and R. Ahlrichs, *Phys. Chem. Chem. Phys.*, 2005, **7**, 3297–3305.
29 F. Neese, *Wiley Interdiscip. Rev.: Comput. Mol. Sci.*, 2022, **12**, e1606.
30 G. Scalmani and M. J. Frisch, *J. Chem. Phys.*, 2010, **132**, 114110.
31 A. Schäfer, C. Huber and R. Ahlrichs, *J. Chem. Phys.*, 1994, **100**, 5829–5835.
32 H. S. Yu, X. He, S. L. Li and D. G. Truhlar, *Chem. Sci.*, 2016, **7**, 5032–5051.
33 M. J. Frisch, G. W. Trucks, H. B. Schlegel, G. E. Scuseria, M. A. Robb, J. R. Cheeseman, G. Scalmani, V. Barone, G. A. Petersson, H. Nakatsuji, X. Li, M. Caricato, A. V. Marenich, J. Bloino, B. G. Janesko, R. Gomperts, B. Mennucci, H. P. Hratchian, J. V. Ortiz, A. F. Izmaylov, J. L. Sonnenberg, D. Williams-Young, F. Ding, F. Lipparini, F. Egidi, J. Goings, B. Peng, A. Petrone, T. Henderson, D. Ranasinghe, V. G. Zakrzewski, J. Gao, N. Rega, G. Zheng, W. Liang, M. Hada, M. Ehara, K. Toyota, R. Fukuda, J. Hasegawa, M. Ishida, T. Nakajima, Y. Honda, O. Kitao, H. Nakai, T. Vreven, K. Throssell, J. A. Montgomery, Jr., J. E. Peralta, F. Ogliaro, M. J. Bearpark, J. J. Heyd, E. N. Brothers, K. N. Kudin, V. N. Staroverov, T. A. Keith, R. Kobayashi, J. Normand, K. Raghavachari, A. P. Rendell, J. C. Burant, S. S. Iyengar, J. Tomasi, M. Cossi, J. M. Millam, M. Klene, C. Adamo, R. Cammi, J. W. Ochterski, R. L. Martin, K. Morokuma, O. Farkas, J. B. Foresman and D. J. Fox, *Gaussian 16 (Revision A.03)*, Gaussian, Inc., Wallingford CT, 2016.
34 M. Linnolahti and S. Collins, *Dalton Trans.*, 2022, **51**, 11152–11162.
35 Y.-P. Li, J. Gomes, S. M. Sharada, A. T. Bell and M. Head-Gordon, *J. Phys. Chem. C*, 2015, **119**, 1840–1850.
36 R. F. Ribeiro, A. V. Marenich, C. J. Cramer and D. G. Truhlar, *J. Phys. Chem. B*, 2011, **115**, 14556–14562.
37 G. Luchini, J. V. Alegre-Requena, Y. Guan, I. Funes-Ardoiz and R. S. Paton, *F1000Research*, 2020, **9**, 291.
38 M. Mammen, E. I. Shakhnovich, J. M. Deutch and G. M. Whitesides, *J. Org. Chem.*, 1998, **63**, 3821–3830.
39 H. H. Brintzinger, D. Fischer, R. Mülhaupt, B. Rieger and R. M. Waymouth, *Angew. Chem., Int. Ed. Engl.*, 1995, **34**, 1143–1170.
40 V. Busico, R. Cipullo, V. Romanelli, S. Ronca and M. Togrou, *J. Am. Chem. Soc.*, 2005, **127**, 1608–1609.
41 L. Sian, A. Dall'Anese, A. Macchioni, L. Tensi, V. Busico, R. Cipullo, G. P. Goryunov, D. Uborsky, A. Z. Voskoboynikov, C. Ehm, L. Rocchigiani and C. Zuccaccia, *Organometallics*, 2022, **41**, 547–560.

